

Article

# Production of Oxide Dispersion Strengthened Mg-Zn-Y Alloy by Equal Channel Angular Pressing of Mechanically Alloyed Powder

Keng-Liang Ou <sup>1,2,3,4</sup> , Chia-Chun Chen <sup>5</sup> and Chun Chiu <sup>5,\*</sup>

<sup>1</sup> Department of Dentistry, Taipei Medical University Hospital, Taipei 110, Taiwan; klouyu@gmail.com

<sup>2</sup> Department of Dentistry, Cathay General Hospital, Taipei 106, Taiwan

<sup>3</sup> Department of Dentistry, Taipei Medical University-Shuang Ho Hospital, New Taipei City 235, Taiwan

<sup>4</sup> 3D Global Biotech Inc., New Taipei City 221, Taiwan

<sup>5</sup> Department of Mechanical Engineering, National Taiwan University of Science and Technology, Taipei 106, Taiwan; chiachun7948@gmail.com

\* Correspondence: cchiu@mail.ntust.edu.tw; Tel.: +886-2-27376479

Received: 8 April 2020; Accepted: 19 May 2020; Published: 21 May 2020



**Abstract:** Mg-Zn-Y alloys with long-period stacking ordered structures (LPSO) have attracted attention due to their excellent mechanical properties. In addition to the LPSO structure, Mg alloys can also be strengthened by oxide particles. In the present study, oxide dispersion strengthened Mg<sub>97</sub>Zn<sub>1</sub>Y<sub>2</sub> (at%) alloys were prepared by equal channel angular pressing (ECAP) of mechanical alloyed (MA) powder under an oxygen gas atmosphere. The 20-h-MA powder had a particle size of 28 μm and a crystallite size of 36 nm. During the MA process followed by ECAP, an Mg matrix with dispersed Y<sub>2</sub>O<sub>3</sub> (and MgO) particles was formed. The alloy processed by ECAP exhibited a hardness of 110 HV and a compressive strength of 185 MPa. Compared to pure Mg, the increased hardness was due to the dispersion strengthening of Y<sub>2</sub>O<sub>3</sub> and MgO particles and solution strengthening of Zn and Y.

**Keywords:** powder metallurgy; mechanical alloying; equal channel angular pressing; dispersion strengthening

## 1. Introduction

Research into light-weight materials is essential to improve fuel efficiency and achieve the goal of energy saving. As one of the most important light-weight structural materials in automotive, aerospace and biomaterial industries, magnesium alloys have drawn much attention because of its high specific strength to weight ratio and recyclability [1–4]. However, the conventional AZ (Mg-Al-Zn) and AM (Mg-Al-Mn) series of Mg alloys will not meet the expanded requirements for load-bearing components [5]. As a result, it is necessary to develop high-performance Mg alloys that will satisfy the extended industrial applications. In recent years, studies have shown that WZ (Mg-Zn-Y) series Mg alloy, which has a long period stacking ordered (LPSO) phase, can improve the mechanical properties of the Mg alloys. As for the fabrication of WZ series alloys, it can be performed by applying the powder metallurgy (P/M) route, which combines powder preparation and consolidation of powders. Mg alloy powders can be produced by rapid solidification such as melt spinning and gas atomization while the consolidation of the alloy powders can be performed by severe plastic deformation (SPD) including hot extrusion and high-pressure torsion (HPT) [6]. Mg<sub>97</sub>Zn<sub>1</sub>Y<sub>2</sub> (at%) alloys were fabricated by a rapidly solidified powder metallurgy (RS/PM) method [7,8]. The bulk alloy prepared by warm extrusion of gas-atomized Mg<sub>97</sub>Zn<sub>1</sub>Y<sub>2</sub> powders exhibited an interesting tensile strength of 610 MPa and modest elongation of 5% in comparison to those of AZ and ZK series Mg alloys prepared by casting. The high

strength was attributed to the presence of the LPSO phase as well as the fine Mg matrix with a grain size of 100–200 nm.

Enhancement of the strength of Mg alloys was also achieved by oxide-dispersion strengthening. Lee et al. reported the compaction of pure Mg powders using equal channel angular pressing (ECAP) [9]. It was observed that MgO was formed during the consolidation process. The sample after four passes of ECAP at 300 °C showed the highest ultimate compressive strength of 193 MPa. The enhanced strength was the result of fine and uniformly-distributed MgO particles. Inspired by the formation of oxide during the compaction process, simultaneous compaction of Mg alloys and oxide dispersion processes was proposed in the present study although the source of oxygen might be from an oxygen gas in the reaction chamber rather than from the oxidizer in the starting materials for an internal oxidation process [10–12]. By introducing oxygen during the compaction process and using an alloying element with a higher oxygen affinity than that of Mg, oxide particles could be formed. The key to the successful internal oxidation of Mg-based alloys is the distribution of oxide. If the oxide could be distributed uniformly in the Mg-matrix rather than agglomerated at the grain boundary region after the compaction, the mechanical property could be enhanced by dispersion strengthening [13].

In addition to direct extrusion of P/M powders, the bulk alloy can be produced by equal channel angular pressing (ECAP) of mechanically-alloyed (MA) powders. Mechanical alloying is a solid-state powder processing technique, in which the welding, fracturing and rewelding of powders are repeated in a ball mill machine to synthesize an alloy [14]. Through the MA process, powders containing super-saturated solid solution, non-equilibrium phase, as well as ultrafine or even monocrystalline grain have been obtained. Zhou et al. synthesized nanocrystalline AZ31-Ti composite by cold pressing of MA powder [15]. After milling for 110 h, a nanocrystalline Mg matrix with a crystallite size of 66 nm was formed. The as-milled AZ31 Mg alloy containing 27 wt% Ti had a hardness of 147 HV, which was three times higher than that of the as-cast AZ31 Mg alloy. Fabrication of Mg<sub>97</sub>Zn<sub>1</sub>Y<sub>2</sub> alloy powder by mechanical alloying of pure Mg, Zn and Y was reported [16]. It was found that peaks of Y and Zn disappeared after milling for 1 h and peaks belonged to Mg<sub>24</sub>Y<sub>5</sub> were identified after 5 h of milling. The crystallite size of the Mg phase was 27 nm. The LPSO phase or oxide phase was not formed after mechanical alloying. The consolidation of the synthesized powder was not reported.

Equal channel angular pressing, one of the severe plastic deformation (SPD) process, was originally developed to prepare bulk alloys with ultrafine structures. In the initial design, the bulk ingot was used as a starting material. In order to obtain nanometer grains, it has been suggested that powders should be used as starting materials. Thus, ECAP processing for the powder was developed. Bulk alloy or composites have been prepared by consolidating alloy or ceramic reinforced metal matrix composite powders using ECAP [17–21]. It has been demonstrated that bulk Cu material having a grain size of less than 100 nm could be prepared by ECAP [22].

In our previous works, Mg<sub>97</sub>Zn<sub>1</sub>Y<sub>2</sub> alloys have been fabricated by stir-casting [23] and by ECAP of mechanically-milled powder (as-cast alloy powder was used as the starting material) under an argon atmosphere [24]. The results showed that the phases existing in the alloy strongly depended on the processing method. Mg<sub>97</sub>Zn<sub>1</sub>Y<sub>2</sub> alloy prepared by casting contained  $\alpha$ -Mg and Mg<sub>12</sub>Zn<sub>1</sub>Y<sub>1</sub> (LPSO phase) while  $\alpha$ -Mg and Mg<sub>24</sub>Y<sub>5</sub> were formed in the alloy prepared by combination of ECAP and mechanical milling. Literature reviews revealed that no prior attempts have been made to study oxide dispersion in Mg-Zn-Y alloy during the ECAP process. It would be interesting to fabricate bulk Mg-Zn-Y alloy by ECAP of mechanically alloyed powder under an oxygen atmosphere. Accordingly, a simultaneous compaction of the Mg alloy and oxide dispersion process was proposed. The aim of the present study was to fabricate bulk Mg<sub>97</sub>Zn<sub>1</sub>Y<sub>2</sub> alloy by ECAP of as-alloyed powders under an oxygen gas atmosphere and to provide early insight into the properties of the compacted bulk alloy. In the present study, elemental Mg, Zn, and Y powders were used as starting materials for mechanical alloying. Microstructure and mechanical properties of the bulk alloy prepared by ECAP of as-alloyed powders were studied to investigate the effect of the ECAP route and pass number on the compaction of powders.

## 2. Materials and Methods

Elemental Mg (99.9%, <45  $\mu\text{m}$ ), Zn (99.9%, <150  $\mu\text{m}$ ) and Y (99.6%, <380  $\mu\text{m}$ ) powders were used as starting materials for preparing  $\text{Mg}_{97}\text{Zn}_1\text{Y}_2$  (at%) alloy powder by the mechanical alloying (MA) process. The stoichiometric ratio of Mg, Zn and Y powder was 97: 1: 2. The powder mixture was milled for 30 h under argon (99.999%) in a planetary ball mill (RETSCH PM100 RETSCH, Haan, Germany). A rotation speed of 250 rpm and a ball-to-powder ratio of 20 were used. To minimize oxidation of the powder, all of the powder handling was performed inside a glove box (homemade) with an argon atmosphere.

For the equal channel angular pressing (ECAP) process, as-milled powders were filled inside a copper tube and compacted by mechanical force, and sealed with a copper cup under an argon-oxygen gas mixture. The sealed tubes were then processed by ECAP at 300 °C. The deformation routes that can be applied in an ECAP process are summarized in Table 1. In the present study, two types of pressing routes including route Bc and route C were selected to investigate the effects of deformation route on microstructure and mechanical properties of the compacted samples. Details of the experimental parameters for the ECAP process can be found elsewhere [24]. The samples were labeled according to their processing route and number of passes. The samples pressed with one pass, two and four pass using route Bc or C were labeled as 1pass, Bc2, Bc4, C2 and C4, respectively.

**Table 1.** Four basic routes that can be applied in a ECAP process.

Route	Process
A	The sample is not rotated.
B <sub>A</sub>	Rotating the sample around its longitudinal axis by 90° clockwise and counterclockwise alternatively
Bc	Rotating the sample around its longitudinal axis after each pass by 90° clockwise
C	Rotating the sample around its longitudinal axis after each pass by 180° clockwise

After the ECAP process, the surrounding Cu tube was removed and density measurements of the compacted samples were performed. The actual density of the sample ( $\rho_a$ ) was measured using the Archimedes method, while the theoretical density ( $\rho_t$ ) was estimated using the rule of mixture. The porosity ( $\Phi$ ) of the sample was estimated using the following equation [25]:

$$\Phi = 1 - \rho_a/\rho_z. \quad (1)$$

A compression test was performed at room temperature using a universal material testing machine MTS810 (MTS, Eden Prairie, MN, USA). Samples with a size of 7.5 mm  $\times$  5 mm  $\times$  5 mm were tested under a strain rate of  $10^{-3}$ /s. Nickel anti-seize paste was used as a lubricant between the sample surface and anvil. Vickers microhardness tests were performed using Akashi MVK-H1 (Mitutoyo, Kawasaki, Japan) microhardness tester. The load and the dwell time were 100 g and 15 s, respectively.

Microstructural characterization was conducted with an optical microscope (OM, OLYMPUS, Tokyo, Japan) and a field-emission scanning electron microscope (FE-SEM) (JEOL JSM-6500F, JEOL, Tokyo, Japan) equipped with energy dispersive spectroscopy (EDS, Oxford Instrument, Abingdon, UK). The particle size distribution of the as-milled powders was measured by a laser particle size analyzer (Malvern Mastersizer 2000, Malvern Panalytical, Malvern, UK). Phase analysis was performed by X-ray diffraction (XRD) (D2 PHASER, Bruker, Madison, WI, USA) using Cu K $\alpha$  radiation. The scan range was from 20° to 90° and the data were collected with a step size of 0.02° and time of 0.5 s. The crystallite size of Mg was calculated from the broadening of the respective XRD peaks. Since the peak broadening is influenced by the crystallite size and microstrain, it is necessary to separate these

two contributions. The separation of crystallite size and strain was obtained from Cauchy/Gaussian approximation using the following equation [26]:

$$\delta^2(2\theta)/\tan^2 \theta = (k\lambda/L)(\delta(2\theta)/\tan \theta \cdot \sin \theta) + 16e^2 \quad (2)$$

$$\delta(2\theta) = B(1 - b^2/B^2) \quad (3)$$

where  $L$  is the mean crystallite size,  $k$  is constant ( $\sim 1$ ) and  $e$  is microstrain.  $\lambda$  is the wavelength and  $\theta$  is the position of the analyzed peak maximum. The term  $\delta(2\theta)$  is used to correct instrumental broadening.  $B$  and  $b$  are the breadths of the XRD peaks of the sample and the reference, respectively.

### 3. Results and Discussion

#### 3.1. Microstructural Characterization

##### 3.1.1. Mechanically-Alloyed Mg-Zn-Y Powders

SEM micrographs of  $Mg_{97}Zn_1Y_2$  powders after mechanical alloying for 1, 10, 20 and 30 h are shown in Figure 1. As shown in the figure, the particle size of the powder decreased continuously when the milling time increased from 1 h to 20 h. After 20 h of milling, an increase of particle size was observed due to the agglomeration between powder particles. The same trend of the evolution of particle size was also obtained by measurement using a particle size analyzer (Figure 2). The particle size of the milled powder decreased from 100  $\mu\text{m}$  to 28  $\mu\text{m}$  when the milling time increased from 1 h to 20 h and then increased to 50  $\mu\text{m}$  when the milling time reached 30 h. XRD-calculated crystallite sizes of Mg decreased from 59 nm to 36 nm when the milling time increased from 1 h to 20 h and then remained almost unchanged when the milling time reached 30 h. The evolution of particle size and crystallite size implied that fracturing and welding of the powders in the milling process had reached equilibrium after milling for 20 h. Thus, the 20-h-milled powder was selected for further compacting by the ECAP process.

XRD analysis was performed to investigate phase evolution during the mechanical alloying process. As shown in Figure 3a, intensities of Mg peaks decreased and became broad with the increase of milling time, indicating the refinement of the crystallite size of the Mg phase. In addition, Mg peaks gradually shifted to a higher diffraction angle. This indicated the lattice parameters of Mg decreased with the increase of milling time, which was confirmed by the calculated lattice parameters of Mg in the MA specimens (Table 2). The dissolution of Zn in Mg will increase the lattice parameters of Mg, while the dissolution of Y will do the opposite. The intensity of the Zn peak decreased as milling time increased, and the Zn peak disappeared after milling for 20 h. In contrast, the Y peak was still observed after milling for 20 h. The results of the XRD analysis indicated that most of Zn dissolved in Mg and only a small portion of Y dissolved after milling for 20 h. The dissolution of Zn was the main factor that resulted in a decrease of the lattice parameters of Mg. The formation of  $Y_2O_3$  was observed after milling for 1 h. After milling for 20 h, peaks belonged to  $\alpha$ -Mg, Y and  $Y_2O_3$  phases were observed. No Mg-Zn-Y, Mg-Y or Mg-Zn intermetallic phases were detected after milling for 20 h. In contrast to the formation of  $Mg_{24}Y_5$  after milling of a mixture of Mg, Zn and Y powder for 5 h in a SPEX mill, which was reported by Koch et al. [16], no Mg-Y intermetallic phases were synthesized in the milled powder in the present work. This was due to the reason that the planetary mill used in the present study had lower mechanical energy than that of the SPEX mill.

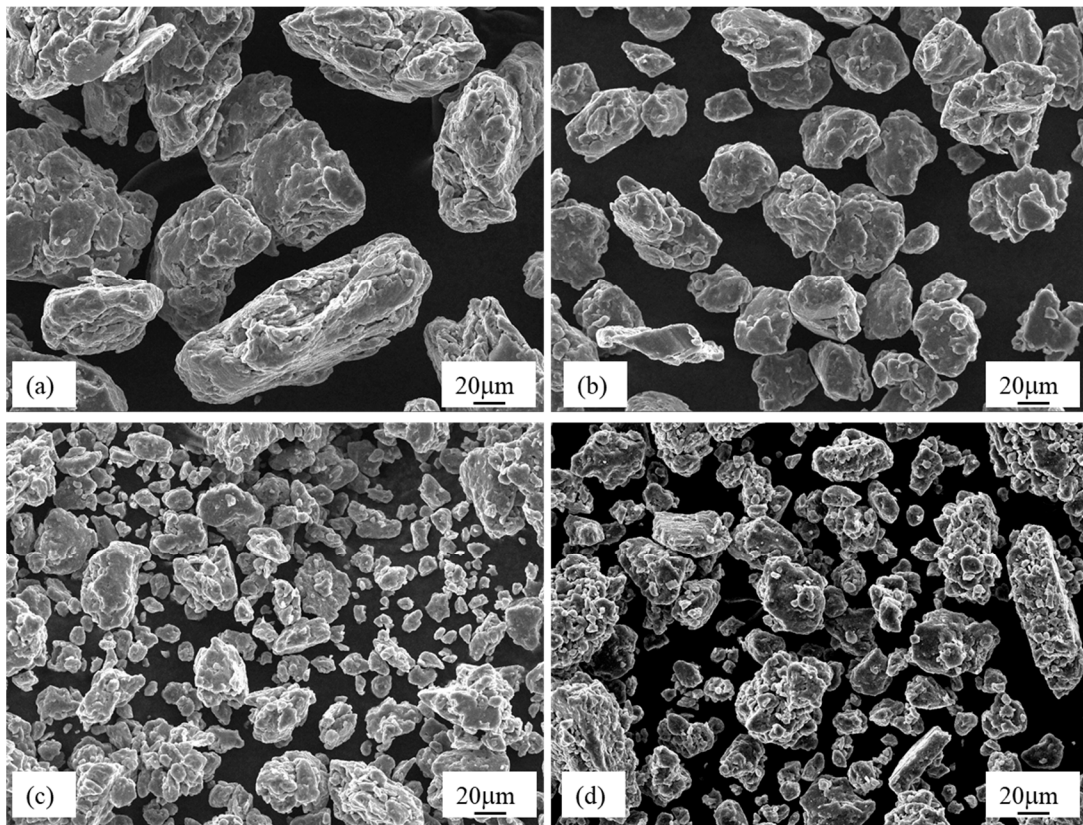


**Figure 1.** Morphology of powder mixture after mechanical alloying for (a) 1 h, (b) 10 h, (c) 20 h and (d) 30 h.

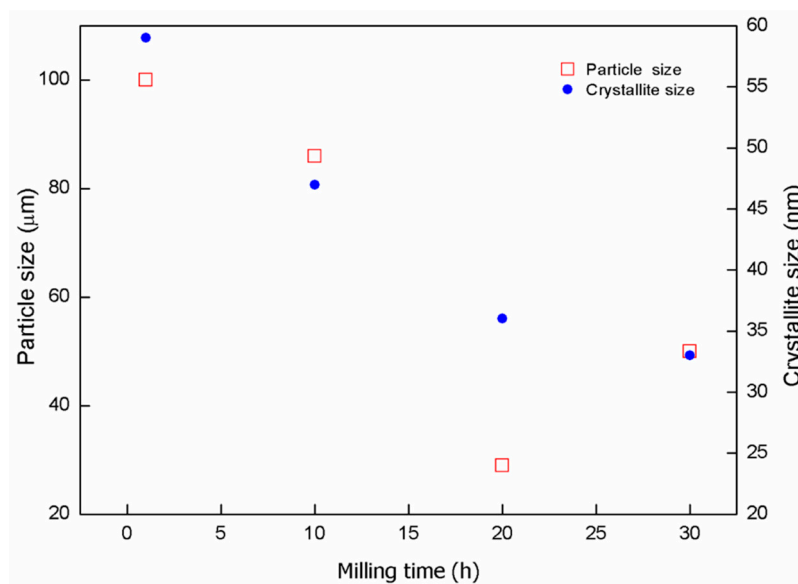


**Figure 2.** Evolution of particle size and crystallite size as a function of milling time.

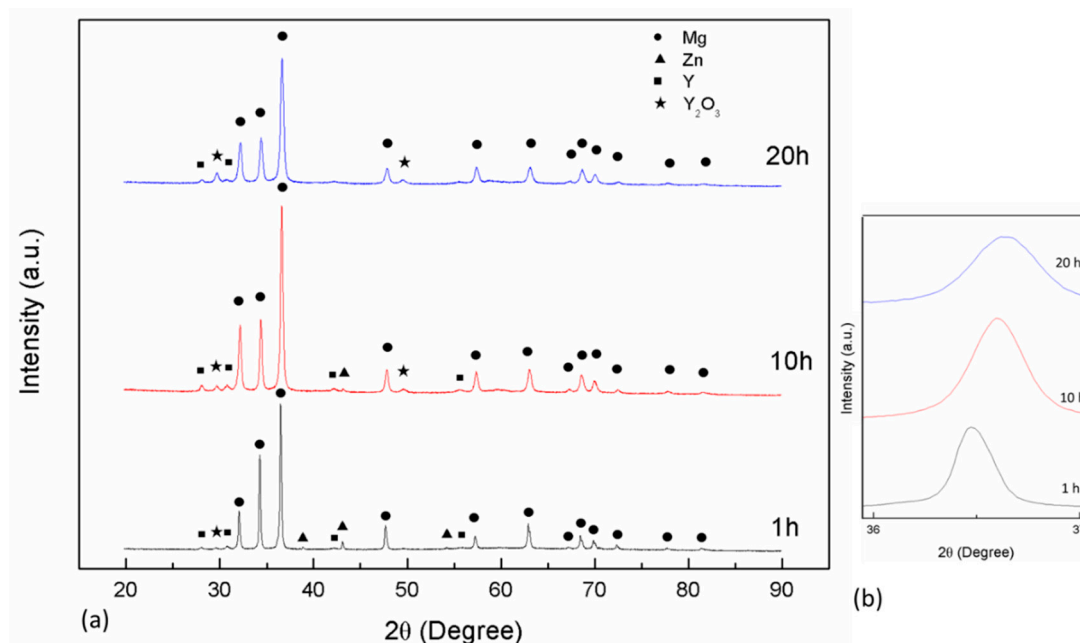


**Figure 3.** XRD patterns of (a)  $Mg_{97}Zn_1Y_2$  alloy after milling for 1 h, 10 h, and 20 h; (b) pattern taken from  $36^\circ$  to  $37^\circ$  showing shifting of (101) Mg peak.

**Table 2.** Particle size, XRD-calculated crystallite size, lattice parameters and unit cell volume of Mg, porosity, and a fraction of oxide in the MA powders after different processing time.

Milling Time (h)	Particle Size ( $\mu\text{m}$ )	Crystallite Size (nm)	Lattice Parameter, a (nm)	Lattice Parameter, c (nm)	Unit Cell Volume ( $10^{-2}\cdot\text{nm}^3$ )
1	100	59	0.3217	0.5223	4.6811
10	86	47	0.3211	0.5212	4.6528
20	29	36	0.3208	0.5208	4.6430
30	50	32	0.3208	0.5207	4.6417

### 3.1.2. Mg-Zn-Y Powders Consolidated by ECAP

XRD patterns of  $Mg_{97}Zn_1Y_2$  powders after compacting with ECAP route Bc or C for one, two and four passes at  $300^\circ\text{C}$  are shown in Figure 4. The pattern of 20-h-milled powder was also included for comparison. After one pass, strong Mg peaks were still observed. The Y peak, which was found in the 20-h-milled sample, disappeared and the intensity of the  $Y_2O_3$  peak increased, indicating the oxidation of retained Y during the ECAP process. The formation of MgO was also observed after one pass. No shifting of Mg peaks was observed, implying the retained Y did not dissolve in Mg but oxidized to form  $Y_2O_3$  during the ECAP process. A further increase in the number of passes or changing ECAP route to route C did not alter the phases presented in the compacted  $Mg_{97}Zn_1Y_2$  samples. No phase transformation occurred when the samples underwent four passes. All of the samples compacted by ECAP route Bc or C contained  $\alpha$ -Mg,  $Y_2O_3$  and MgO phase. In the present work, the number of passes and route had no effect on the formation of phases in the consolidated bulk samples. There was no formation of binary Mg-Y and Mg-Zn or ternary Mg-Zn-Y phases after ECAP. During the MA process, part of the Y in the powder oxidized and formed  $Y_2O_3$ . In the following ECAP process, the retained Y reacted with oxygen and the formation of  $Y_2O_3$  was completed. The results showed that an Mg alloy with dispersed  $Y_2O_3$  particles was successfully synthesized during MA and the followed ECAP process.

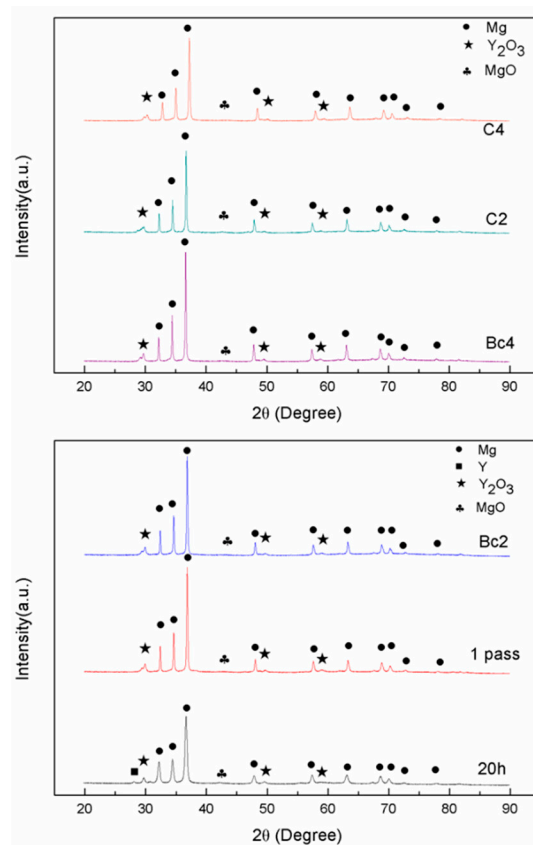


**Figure 4.** XRD patterns of powder after compacting by ECAP route C and Bc for one, two and four pass. The pattern of the 20-h-milled sample is also included for comparison.

Crystallite size of Mg increased from 36 nm in the 20-h-milled sample to 77 nm in the sample after one pass of ECAP route Bc and decreased to 64 nm when the number of passes increased to four. The observation that crystallite growth after one pass of ECAP at 300 °C and refinement after four passes agreed with the reported results that the ECAP process was able to refine the grain size when the number of passes increased [27]. The refinement of crystallite size was not observed in the samples processed with ECAP route C. The refinement seemed to be impeded by the oxide layer in the outer region of the sample.

Microstructures of the  $Mg_{97}Zn_1Y_2$  powder samples consolidated by ECAP route Bc are shown in Figure 5. The one-pass sample consisted of three zones. EDS analysis results indicated that matrix (zone 1) was an Mg-rich phase (99.75 at% Mg, 0.24 at% Zn and 0.01 at% Y). In comparison to the matrix, dispersed particle (zone 2) was richer in Y and O (42.07 at% Mg, 31.12 at% Y and 26.81 at% O). A grey layer presented on the particle surfaces (zone 3) was an Mg-rich and O-rich phase (64.08 at% Mg and 35.93 at% O). Combining the results from the XRD and EDS analyses, it was concluded that the one-pass sample consisted of  $\alpha$ -Mg (a solid solution containing a small amount of Zn and Y), dispersed  $Y_2O_3$  particles and an MgO layer presented on the particle surfaces. After two passes, particles richer in Mg and O were identified in the Mg-matrix, indicating the oxide layer on the particle surface had been broken into particles. ECAP effectively broke down the MgO layer into small particles during the process. Compared to the two-pass sample, the composition of these three zones remained almost unchanged after four passes. This indicated that no phase transformation occurred after four passes. Porosities were also observed. The porosity of the one-pass, two-pass and four-pass samples was 9.7%, 7.6%, and 4.3%, respectively. The powder could be compacted more densely by the Bc route with the increasing number of passes.

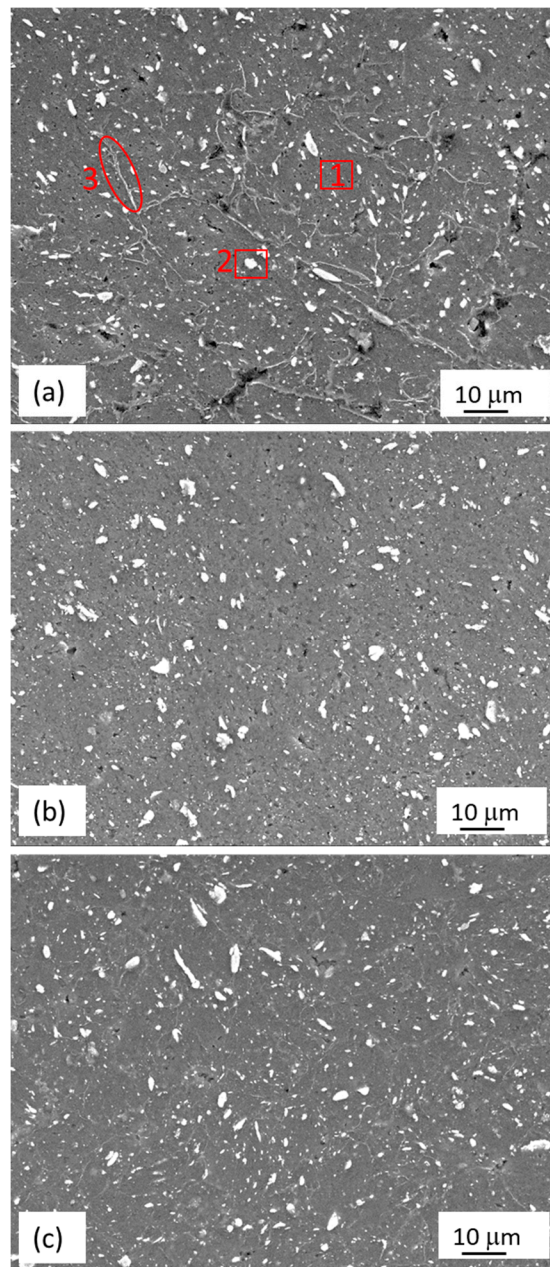


**Figure 5.** SEM micrograph of powder after compacting by ECAP route Bc for (a) one pass, (b) two passes and (c) four passes.

Figure 6a,b shows the microstructures of the powder samples pressed by route C for two and four passes, respectively. Similar to the powder compacted by route Bc, the samples pressed by route C also contained  $\alpha$ -Mg, MgO and  $Y_2O_3$  phases. However, the distribution of MgO was different in the inner and outer region in samples processed by route C. For the samples pressed by route C, MgO presented as dispersed particles in the  $\alpha$ -Mg matrix in the inner portion of the sample (Figure 6a,b), while MgO was shown as a layer between Mg particles in the outer portion of the sample (Figure 6c). A clear boundary between the inner and outer zone could be observed (Figure 6d). The particles in the inner zone were compacted more effectively than those in the outer zone since the oxide layer has been broken into particles. The sample compacted by route C for four passes had a porosity of 8.1% while the sample compacted by route Bc for four passes had a porosity of 4.3%. The porosity of the sample

pressed by route C was higher than that of the sample compacted by route Bc. No binary Mg-Zn, Mg-Y or ternary Mg-Zn-Y phases have been formed after the ECAP process.

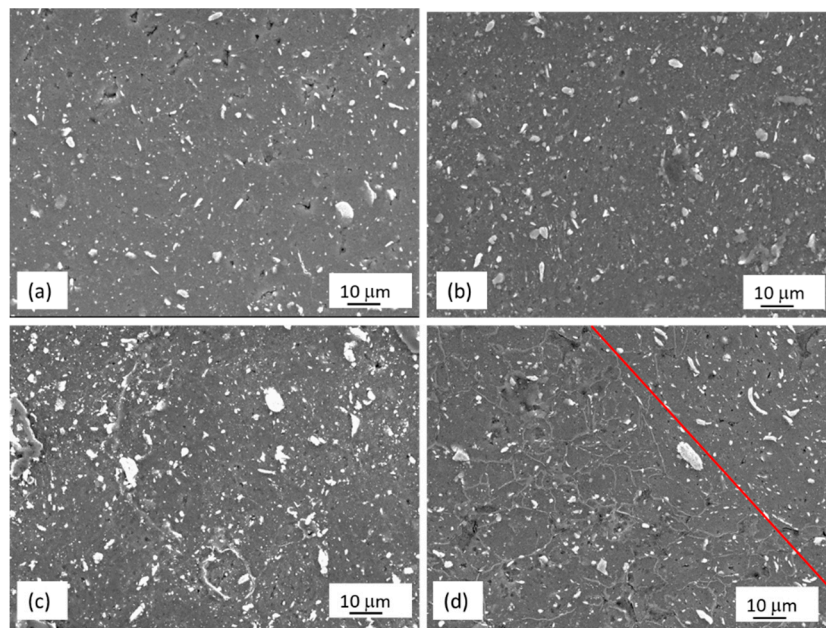


**Figure 6.** SEM micrograph of powder after compacting by ECAP route C for (a) two passes and (b) four passes; (c) outer zone of powder compacted by ECAP route C and (d) interface for interior and outer zone.

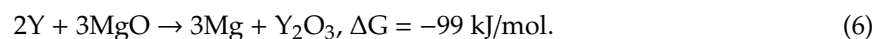
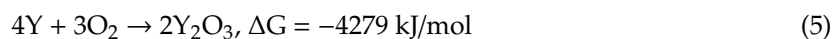
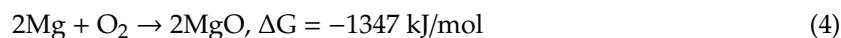
Shearing characteristics in an ECAP process can be discussed with shear patterns in three orthogonal planes of observation. The plane X was the mutually orthogonal plane of sectioning lying perpendicular to the longitudinal axis of the sample, while planes Y and Z were planes parallel either to the side faces or to the top face of the sample at the point of exit from the die, respectively [28]. Samples pressed using route C had deformation in the X and Y planes but no deformation in the Z plane. Samples compacted by route Bc had continuous deformation in three planes. Moreover, the strain path got reversed in the successive passes, enabling the easy formation of shear bands [29]. Thus, the samples pressed by route Bc had a higher compacting efficiency and lower porosity. The nonuniform distribution of shear force in the Z plane resulted in different morphology of MgO in the inner and outer region in the sample pressed by ECAP route C.

The fraction of oxide in the compacted samples was between 12.1% and 13.2% (Table 3), indicating the number of passes and type of route had no effect on the fraction of oxide. Most of the oxidation was completed after one pass of ECAP. No refinement of the crystallite size of Mg was observed in the present work. The porosity of the sample compacted by route Bc decreased from 9.7% after one pass to 4.3% after four passes (Table 3).

**Table 3.** XRD-calculated crystallite size of Mg, porosity and fraction of oxide in the ECAPed samples.

Route and Pass	Crystallite Size (nm)	Porosity (%)	Fraction of Oxide (%)
1 Pass	77	9.7	12.4
Bc 2	67	7.6	13.2
Bc 4	64	4.3	12.0
C2	73	9.2	12.1
C4	73	8.1	13.4

In the present work, the synthesis of  $Y_2O_3$  reinforced Mg alloys during the MA and the subsequent ECAP process was achieved. The possible oxidation reactions and calculated Gibbs free energy of the reactions in a system with Mg, Y and O were as follows [30]:



According to Reactions (4) and (5), the formation motivation of  $Y_2O_3$  was quite higher than that of MgO. Thus, the oxidation of Y in the Mg matrix was possible during the MA and the subsequent ECAP process. It was also possible that  $Y_2O_3$  formed via Reaction (6) during the process.

### 3.2. Mechanical Properties

Table 4 lists Vickers microhardness of  $Mg_{97}Zn_1Y_2$  powder compacted by ECAP route Bc or C at 300 °C. The Vickers hardness was in the range of 100 to 110 Hv. The type of route and number of passes did not show a strong effect on the hardness of compacted samples. Pure Mg powder after compacting at 300 °C by ECAP using route Bc for four times exhibited a hardness of 49 Hv [9]. As-cast  $Mg_{97}Zn_1Y_2$  had a hardness of ~80 Hv [24]. As shown in Table 4, hardness values of the  $Mg_{97}Zn_1Y_2$  powders compacted by ECAP at the present work were higher than those of compacted Mg powder and as-cast  $Mg_{97}Zn_1Y_2$  ingot. The increase of hardness was due to the solid solution of Zn and Y, and the dispersion of oxides; the latter was the dominant factor.

**Table 4.** Vickers hardness, compressive strength and failure strain of ECAPed samples.

Route and Pass	Hardness (HV)	Compressive Strength (MPa)	Failure Strain (%)
1 Pass	101	67	8
Bc 2	101	90	3
Bc 4	110	185	4
C2	103	60	6
C4	100	44	1

The results of compressive tests for  $Mg_{97}Zn_1Y_2$  compacted by ECAP route Bc and C for one, two, and four passes at 300 °C are summarized in Table 4. After one pass, the ultimate compressive strength (UCS) of the compacted sample reached 67 MPa and failure strain was 8%. After two passes of route Bc, UCS increased to 90 MPa, and failure strain decreased to 3%. A further increase in the pass number to four passes resulted in an increase in UCS (185 MPa). In contrast, UCS and failure strain of the sample after two passes of route C remained close to those of the one-pass sample. Moreover, those values even decreased after four passes of route C. UCS of the four-pass sample was lower than that of the pure Mg sample (190 MPa).

The strength of the compacted samples could be affected by the grain size of the matrix, particle size and fraction of dispersed phase, and porosity. In the present study, the fraction and size of the oxide phase remained almost unchanged for the compacted samples produced by ECAP routes C and Bc for one, two and four passes (Table 3). Therefore, they were not the dominant factors affecting the mechanical properties of the compacted samples. The XRD-calculated crystallite size and porosity decreased with the increasing number of passes in samples processed with route Bc. However, they remained almost the same in samples processed with route C. The sample pressed with route Bc for four passes possessed both of the finest crystallite size and the lowest porosity. Thus, the UCS of the sample after four ECAP passes with route Bc was enhanced but the failure strain was sacrificed as compared to the one-pass sample. Moreover, the distribution of the oxide (MgO) layer at the outer region of samples processed with route C also resulted in a lower UCS than those of samples compacted

with route Bc. Unlike the dispersed oxide particles in the inner portion of the sample, these oxide layers lowered the bonding of the powders.

Compared to the UCS of compacted Mg samples reported by Lee et al. using the same ECAP parameters [9], the UCS of the samples in the present work was not enhanced even with the dispersion of  $Y_2O_3$ . This was due to the higher amount of porosity in the present work (4.3% in the present work in comparison to 1.6% in the pure Mg sample [9]). However, the hardness value was higher than that of the pure Mg sample. The reason was that Vickers hardness was measured in a small area with a minimal effect of porosity. On the other hand, the results obtained from the compression test were affected strongly by the presence of porosity.

Feasibility of simultaneous synthesis of dispersed  $Y_2O_3$  particles and compaction of Mg alloy powders during MA and followed ECAP process was confirmed in the present study. However, the processing parameters needed to be optimized to improve the mechanical properties of the compacted Mg alloy samples in future work. Mallick et al. studied the deformation behavior of Mg-2vol.% $Y_2O_3$  nanocomposite [31]. The composite was fabricated using the powder metallurgy (PM) method, including powder blending of pure Mg and  $Y_2O_3$  powder (particle size of 30–50 nm), cold compaction, sintering and hot extrusion. The extruded sample had a strength of 291 MPa, which was higher than ours. In addition to decreasing the high porosity, the particle size of  $Y_2O_3$  should be reduced and the fraction of  $Y_2O_3$  needs to be optimized to improve the strength of the compacted samples.

#### 4. Conclusions

In the present study, a bulk  $Mg_{97}Zn_1Y_2$  alloy reinforced by  $Y_2O_3$  particles was prepared by simultaneous synthesizing  $Y_2O_3$  particles and compacting mechanically-alloyed powders using equal channel angular pressing. The main conclusions can be summarized as follows:

1. The  $Mg_{97}Zn_1Y_2$  alloy powder after mechanical alloying for 20 h consisted of  $\alpha$ -Mg, Y and  $Y_2O_3$  phases. The ECAP-compacted bulk alloy contained the  $\alpha$ -Mg matrix, uniformly dispersed  $Y_2O_3$  and MgO phase.
2. The powder compacted with ECAP route Bc for four passes exhibited a hardness of 110 HV and an ultimate compressive strength of 185 MPa. The hardness was higher than those of as-cast  $Mg_{97}Zn_1Y_2$  alloy and compacted Mg; however, the UCS was lower.
3. The improved hardness observed in the ECAP-compacted alloy was mainly attributed to the dispersion hardening of  $Y_2O_3$  particles. The decrease in ultimate compressive strength was due to the higher amount of porosity in the ECAP-compacted alloy.

**Author Contributions:** Conceptualization, K.-L.O. and C.C.; Validation, C.C.; Formal Analysis, C.-C.C. and C.C.; Investigation, K.-L.O., C.-C.C. and C.C.; Writing-Original Draft Preparation, C.C.; Funding Acquisition, K.-L.O. All authors have read and agreed to the published version of the manuscript.

**Funding:** This research was funded by the Taipei Medical University and National Taiwan University of Science and Technology in Taiwan under TMU-NTUST joint research program contract no. TMU-NTUST-104-11.

**Acknowledgments:** The authors would like to thank Sheng-Chuan Liao (PIC, NTUST) for the technical support on SEM-EDS analysis.

**Conflicts of Interest:** The authors declare no conflict of interest.

#### References

1. Mordike, B.L.; Ebert, T. Magnesium: Properties-applications-potential. *Mater. Sci. Eng. A* **2001**, *302*, 37–45. [[CrossRef](#)]
2. Schumann, S. The paths and strategies for increased magnesium applications in vehicles. *Mater. Sci. Forum* **2005**, *488*, 1–8. [[CrossRef](#)]
3. Cabibbo, M.; Spigarelli, S. A TEM quantitative evolution of strengthening in an Mg-RE alloy reinforced with SiC. *Mater. Charact.* **2011**, *62*, 959–969. [[CrossRef](#)]

4. Pan, F.S.; Yang, M.B.; Chen, X.H. A review on casting magnesium alloys: Modification of commercial alloys and development of new alloys. *J. Mater. Sci. Technol.* **2016**, *32*, 1211–1221. [[CrossRef](#)]
5. You, S.; Huang, Y.; Kainer, K.U.; Hort, N. Recent research and developments on wrought magnesium alloys. *J. Magnesium Alloys* **2017**, *5*, 239–253. [[CrossRef](#)]
6. Figueiredo, R.B.; Langdon, T.G. Processing Magnesium and Its Alloys by High-Pressure Torsion: An Overview. *Adv. Eng. Mater.* **2019**, *21*, 1801039. [[CrossRef](#)]
7. Kawamura, Y.; Hayashi, K.; Inoue, A.; Masumoto, T. Rapidly solidified powder metallurgy Mg<sub>97</sub>Zn<sub>1</sub>Y<sub>2</sub> alloy with excellent tensile yield strength above 600 MPa. *Mater. Trans.* **2001**, *42*, 1172–1176. [[CrossRef](#)]
8. Inoue, A.; Matsushita, M.; Kawamura, Y.; Amiya, K.; Hayashi, K.; Koike, J. Novel hexagonal structure of ultra-high strength magnesium-based alloys. *Mater. Trans.* **2002**, *43*, 580–584. [[CrossRef](#)]
9. Lee, H.C.; Chao, C.G.; Liu, T.F.; Lin, C.Y.; Wang, H.C. Effect of temperature and extrusion pass on the consolidation of magnesium powders using equal channel angular extrusion. *Mater. Trans.* **2013**, *54*, 765–768. [[CrossRef](#)]
10. Li, G.; Sun, J.; Guo, Q.; Wang, R. Fabrication of the nanometer Al<sub>2</sub>O<sub>3</sub>/Cu composite by internal oxidation. *J. Mater. Process. Tech.* **2005**, *170*, 336–340. [[CrossRef](#)]
11. Broyles, S.E.; Anderson, K.R.; Groza, J.R.; Gibeling, J.C. Creep deformation of dispersion-strengthened copper. *Metall. Mater. Trans A* **1996**, *27*, 1217–1227. [[CrossRef](#)]
12. Rapp, R.A. Kinetics, Microstructures and mechanism of internal oxidation—Its effect and prevention in high temperature alloy oxidation. *Corrosion* **1965**, *21*, 382–401. [[CrossRef](#)]
13. Chino, Y.; Furuta, T.; Hakamada, M.; Mabuchi, M. Influence of distribution of oxide contaminants on fatigue behavior in AZ31 Mg alloy recycled by solid-state processing. *Mater. Sci. Eng. A* **2006**, *424*, 355–360. [[CrossRef](#)]
14. Suryanarayana, C. Mechanical alloying and milling. *Prog. Mater. Sci.* **2001**, *46*, 1–184. [[CrossRef](#)]
15. Zhou, H.; Hu, L.; Sum, Y.; Zhang, H.; Duan, C.; Yu, H. Synthesis of nanocrystalline AZ31 magnesium alloy with titanium addition by mechanical milling. *Mater. Charact.* **2016**, *113*, 108–116. [[CrossRef](#)]
16. Koch, C.C.; Scattergood, R.O.; Youssef, K.M.; Chan, E.; Zhu, Y.T. Nanostructured materials by mechanical alloying: New results on property enhancement. *J. Mater. Sci.* **2010**, *45*, 4725–4732. [[CrossRef](#)]
17. Senkov, O.N.; Miracle, D.B.; Scott, J.M.; Senkova, S.V. Compaction of amorphous aluminum alloy powder by direct extrusion and equal angular extrusion. *Mater. Sci. Eng. A* **2005**, *393*, 12–21. [[CrossRef](#)]
18. Kim, H.S.; Seo, M.H.; Oh, C.S.; Kim, S.J. Equal channel pressing of metallic powders. *Mater. Sci. Forum* **2003**, *437*, 89–92. [[CrossRef](#)]
19. Nagasekhar, A.V.; Yip, T.H.; Ramakanth, K.S. Mechanics of single pass equal channel angular extrusion of powder in tubes. *Appl. Phys. A* **2006**, *85*, 185–194. [[CrossRef](#)]
20. Baker, I.; Iliescu, D.; Liao, Y. Containerless consolidation of Mg powders using ECAE. *Mater. Manuf. Processes* **2010**, *25*, 1381–1384. [[CrossRef](#)]
21. Nagasekhar, A.V.; Yip, T.H.; Guduru, R.K.; Ramakanth, K.S. Multipass equal channel angular pressing of MgB<sub>2</sub> powder in tubes. *Physica C* **2007**, *466*, 174–180. [[CrossRef](#)]
22. Karaman, I.; Haouaoui, M.; Maier, H.J. Nanoparticle consolidation using equal channel angular extrusion at room temperature. *J. Mater. Sci.* **2007**, *42*, 1561–1576. [[CrossRef](#)]
23. Chiu, C.; Lu, C.; Chen, S.; Ou, K. Effect of Hydroxyapatite on the Mechanical Properties and Corrosion Behavior of Mg-Zn-Y Alloy. *Materials* **2017**, *10*, 885. [[CrossRef](#)] [[PubMed](#)]
24. Chiu, C.; Huang, H. Microstructure and properties of Mg-Zn-Y alloy powder compacted by equal channel angular pressing. *Materials* **2018**, *11*, 1678. [[CrossRef](#)] [[PubMed](#)]
25. Ramya, M.; Sarwat, S.G.; Udhayabanu, V.; Subramanian, S.; Raj, B.; Ravi, K.R. Role of partially amorphous structure and alloying elements on the corrosion behavior of Mg-Zn-Ca bulk metallic glass for biomedical applications. *Mater. Des.* **2015**, *86*, 829–835. [[CrossRef](#)]
26. Klug, H.P.; Alexander, L. *X-ray Diffraction Procedures for Polycrystalline and Amorphous Materials*, 2nd ed.; John Wiley & Sons: New York, NY, USA, 1974; pp. 618–708.
27. Figueiredo, R.B.; Langdon, T.G. Grain refinement and mechanical behavior of a magnesium alloy processed by ECAP. *J. Mater. Sci.* **2010**, *45*, 4827–4836. [[CrossRef](#)]
28. Furukawa, M.; Iwahashi, Y.; Horita, Z.; Nemoto, M.; Langdon, T.G. The shearing characteristics associated with equal-channel angular pressing. *Mater. Sci. Eng. A* **1998**, *257*, 328–332. [[CrossRef](#)]

29. Iwahashi, Y.; Horita, Z.; Nemoto, M.; Langdon, T.G. An investigation of microstructural evolution during equal-channel angular pressing. *Acta Mater.* **1997**, *45*, 4733–4741. [[CrossRef](#)]
30. Barin, I. *Thermochemical Data of Pure Substance*, 3rd ed.; VCH Publishers: New York, NY, USA, 1995; p. 993.
31. Mallick, A.; Tun, K.S.; Gupta, M. Deformation behavior of Mg/Y<sub>2</sub>O<sub>3</sub> nanocomposite at elevated temperatures. *Mater. Sci. Eng. A* **2012**, *551*, 222–230. [[CrossRef](#)]



© 2020 by the authors. Licensee MDPI, Basel, Switzerland. This article is an open access article distributed under the terms and conditions of the Creative Commons Attribution (CC BY) license (<http://creativecommons.org/licenses/by/4.0/>).